The International Journal of Advanced Manufacturing Technology (2018) 99:3091–3109
https://doi.org/10.1007/s00170-018-2611-8

ORIGINAL ARTICLE

Effects of the physicochemical properties of different nanoparticles on lubrication performance and experimental evaluation in the NMQL milling of Ti–6Al–4V

Qingan Yin[1] · Changhe Li[1] · Lan Dong[2] · Xiufang Bai[2] · Yanbin Zhang[1] · Min Yang[1] · Dongzhou Jia[1] · Yali Hou[1] · Yonghong Liu[3] · Runze Li[4]

Received: 11 May 2018 / Accepted: 16 August 2018 / Published online: 19 September 2018

Abstract

Processing of Ti alloy is often accompanied with large frictions and high temperature. Nanofluids prepared by adding nanoparticles show good lubrication performance due to the excellent antifriction and antiwear of nanoparticles. The physicochemical properties of nanoparticles are important factors that influence the lubrication performance of nanofluid minimum quantity lubrication (NMQL). An experimental study on Ti alloy (Ti–6Al–4V) milling was conducted to explore the lubrication performance of minimum quantity lubrication (MQL) using different nanofluids. Cottonseed oil was used as the base oil, and the tribological properties of several typical nanoparticles (i.e., Al_2O_3, MoS_2, SiO_2, carbon nanotubes, SiC, graphite) were studied. The lubrication performance was evaluated by milling parameters, including milling force, surface roughness (R_a, RS_m, R_{mr}), friction coefficient, microstructures of debris and workpiece surface, and energy spectra of the workpiece surface. Results demonstrated that the milling process based on Al_2O_3 nanofluid achieved the minimum milling force and friction coefficient, whereas the milling process based on SiO_2 nanofluid had the minimum surface roughness value (R_a). Furthermore, the physicochemical properties of nanoparticles and the viscosity of nanofluid were analyzed. Spherical Al_2O_3 and SiO_2 nanoparticles improved the lubrication effect of base oil mostly. The Al_2O_3 nanoparticles exhibited high hardness, which was conducive to reducing milling force. SiO_2 nanofluid demonstrated high viscosity, which could improve workpiece surface quality.

1. Milling performance of Ti–6Al–4V under different lubricating conditions was studied.
2. The tribological properties of several typical nanoparticles were studied.
3. Physicochemical properties of different nanoparticles were analyzed.
4. Viscosity of different nanofluids was analyzed to validation.
5. The best workpiece surface quality was obtained by SiO_2 NMQL.

✉ Changhe Li
sy_lichanghe@163.com

✉ Yonghong Liu
liuyh@upc.edu.cn

Qingan Yin
15154215806@163.com

Lan Dong
804203464@qq.com

Xiufang Bai
1104024833@qq.com

Yanbin Zhang
zhangyanbin1_qdlg@163.com

Min Yang
yummy0lige@163.com

Dongzhou Jia
jia_dongzhou@163.com

Yali Hou
510601951@qq.com

Runze Li
runzeli@usc.edu

[1] School of Mechanical and Automotive Engineering, Qingdao University of Technology, Qingdao 266520, China

[2] School of Mechanical and Electrical Engineering, Qingdao Binhai University, Qingdao 266555, China

[3] College of Mechanical and Electronic Engineering, China University of Petroleum (East China), Qingdao 266580, China

[4] Department of Biomedical Engineering, University of Southern California, Los Angeles, CA 90089–1111, USA

Keywords Minimum quantity lubrication · Nanoparticles · Cottonseed oil · Ti alloy · Milling · Tribological properties

Nomenclature

MQL	Minimum quantity lubrication
NMQL	Nanofluid minimum quantity lubrication
SEM	Scanning electron microscope
EDS	Energy-dispersive spectrometer
W_s	Rotation rate (r/min)
V_f	Feed rate (mm/min)
V	Cutting speed
a_p	Radial depth of cut (mm)
a_e	Axial depth of cut (mm)
α	Angle of nozzle and tool feeding direction
β	Angle of nozzle and horizontal direction
t	Processing time
F_x,F_y, F_z	Cutting force component in X, Y, and Z directions (N)
F_t, F_r	Tangential and radial cutting force components (N)
F	Resultant cutting force (N)
$\overline{F}_{max}$	Mean of milling force peak
R_a	Arithmetic average height (μm)
RS_m	Mean spacing at mean line (mm)
R_z	Maximum height of profile
R_{mr}	Bearing length ratio
Q_w	Volume of material removed by tool
P	Total energy consumed
μ	Friction coefficient
γ	Cut in angle
μ_n	Viscosity of nanofluid
μ_{bf}	Viscosity of base fluid
φ	Nanoparticle volume fraction

1 Introduction

Ti alloy is extensively used in the aerospace industry due to its high strength and antiwear [1]. This alloy is an important metal part in airplane structures and engine parts [2]. However, the cutting zone is accompanied with great frictions and high temperature and pressure due to the difficulty of machining Ti alloy, which determines the extremely important role of lubrication in tool–workpiece interface during the processing [3, 4]. Cutting fluid is vital to the processing. This fluid is mainly responsible for avoiding workpiece burning, decreasing tool–workpiece surface friction, and eliminating debris [5–7]. However, the use of cutting fluid causes many problems, including environmental and water pollutions and threats to operators' safety [8]. Environmental production, energy saving, and emission reduction have attracted significant attention from the public [9]. Minimum quantity lubrication (MQL) has been developed at the right moment to address these problems [10, 11].

MQL has shown considerable advantages and development prospects in replacing the traditional flood [12, 13]. The heat transfer capability of solids is considerably stronger than that of liquid and gas [14, 15]; a certain amount of nanosolid particles is added to trace lubricant to form nanofluid for improving the heat transfer capability and lubrication performance of MQL [16, 17]. Ding et al. [18, 19] investigated the removal mechanism of brittle particles in mechanical machining. Mao [20–22] and Li et al. [23–26] confirmed the excellent cooling and lubrication effects of nanofluid minimum quantity lubrication (NMQL). The application of nanofluid in MQL processing not only inherits all the advantages of MQL milling but also solves the fatal defect of the insufficient heat transfer ability in MQL milling.

Considerable research on MQL using different nanofluids has been reported. For Al_2O_3 nanoparticles, Hadi and Atefi [27] investigated the effect of Al_2O_3 NMQL in the milling processes of AISID3 steel and found that the surface roughness was 25% lower than that of pure MQL. Shen et al. [28] grinded cast iron with Al_2O_3 and diamond nanofluids. The process was compared with dry, pouring, and MQL grinding. NMQL reduced the grinding force and surface roughness considerably and eliminated workpiece burn. Mao et al. [20, 29] compared grinding performance under dry, flood, MQL, and Al_2O_3 NMQL conditions. Experimental results demonstrated that NMQL achieved low grinding force and grinding temperature and a better workpiece surface quality. Yin et al. [30] proved that Al_2O_3 NMQL had the lowest force and friction coefficient in milling 45 steel.

For MoS_2 nanoparticles, Shen et al. [31] and Kalita et al. [32] obtained excellent performance of MoS_2 nanoparticles in improving grinding force. Rahmati et al. [33, 34] studied the surface morphology of MoS_2 nanoparticle end-milling Al 6061-T6 workpiece with different concentrations. The best workpiece surface quality was obtained by 0.5 wt% MoS_2 nanoparticle milling. Uysal et al. [35] used different flow rates (20 and 40 ml/h) of MoS_2 nanoscale fluid to cut stainless steel and determined that minimum initial tool wearing and surface roughness were acquired under 40 ml/h nanofluid flow rate. Dilbag et al. [36] studied the turning performance of different lubrication conditions (dry, graphite NMQL, and MoS_2 NMQL) and identified that MoS_2 NMQL contributed the best workpiece surface quality.

For SiO_2 nanoparticles, Ming et al. [37] and Sayuti et al. [38, 39] used SiO_2 nanofluid end-milling Al6061-T6. The results showed that SiO_2 nanoparticles reduced cutting force and improved the workpiece surface quality. Peng et al. [40] found that SiO_2 NMQL had lower friction coefficient and tool

wear than diamond NMQL. Sarhan et al. [41] concluded that SiO_2 nanoparticles could remarkably reduce the friction coefficient of tool–debris interface, thereby reducing cutting force and power. For carbon nanotubes (CNTs) nanoparticles, CNTs have been widely studied due to their high heat conductivity and extremely high surface ratio. They possess potential application prospects in different fields due to their unique electrical, thermal, and mechanical properties [42]. Zhang et al. [43] used MoS_2, carbon nanotube (CNT), and ZrO_2 nanoparticles as additives of grinding fluid to perform grinding experiments. The results demonstrated that MoS_2 nanoparticles achieved the lowest specific energy and the best workpiece surface quality.

For SiC nanoparticles, Jia et al. [44] proved their good tribological properties. Zhang et al. [45, 46] mixed Al_2O_3 and SiC nanoparticles. The influences of different mixing ratios and grain sizes on the lubrication performance were discussed. The best lubrication performance was achieved under 2:1 mixing ratio and 30:70 grain size ratio. For graphite nanoparticles, Lee et al. [47] and Alberts et al. [48] proved that they presented excellent performance in reducing friction coefficient, temperature, and surface roughness. Huang et al. [49] and Shaji et al. [50, 51] showed that the addition of flake graphite to cutting fluid could substantially reduce cutting force, friction coefficient, and surface roughness.

Nevertheless, different nanoparticles have different physicochemical properties, which determine their dissimilar tribological properties [52]. Therefore, the antifriction and antiwear of different nanoparticles must be discussed. Although scholars have conducted abundant studies on NMQL, the effects of the physicochemical properties of different nanoparticles on MQL performance have not been discussed deeply. Hence, six types of nanofluids and pure base oil were used in Ti alloy milling experiment. Milling force, friction coefficient, surface roughness, microstructures of debris and workpiece surface, and energy spectrum of the workpiece surface under the use of different nanofluids were studied. Furthermore, the physicochemical properties of different nanoparticles and the viscosity of nanofluid were analyzed, which disclosed the tribological properties of different nanoparticles and realized a low-carbon green production with the characteristics of high efficiency, low-energy consumption, environmental protection, and resource saving.

2 Experimental

2.1 Experimental setup

The experiment was performed on a Dema ML1060B CNC milling machine. Table 1 presents the parameters of the milling machine. The overall dimension was 3200 mm × 2450 mm × 2000 mm (L × W × H). The technological parameters mainly included the following: principal axis power = 11 kW, maximum speed = 8000 r/min, motor power driving the workbench = 5 kW, cutting range = 1000 mm × 600 mm × 600 mm, and cutting feed rate = 10,000 mm/min. Minimum lubrication oil was transmitted using a JinZhao KS-2106 MQL system. During data collection, three-phase milling force was measured using a piezoelectric three-phase measuring dynamometer (the sampling frequency was 30,000 Hz). Surface roughness was measured using a TIME3220 contact pointer measuring device (five points were selected under each working condition to collect and record data). Debris was collected at the end of each experiment. Debris and workpiece microstructure and elemental analysis were conducted using a DV2TLV scanning electron microscope (SEM). The viscosity of nanofluids was measured using a Brookfield DV2T viscometer. Figure 1 shows the experimental and analysis equipment.

Table 1 Parameters of Dema ML1060B CNC milling machine

Machine parameters	Value
Principal axis power	11 kW
Motor power driving the workbench	5 kW
Highest rotating speed	8000 r/min
Cutting range	1000 mm × 600 mm × 600 mm
Cutting feed rate	10,000 mm/min

2.2 Experimental materials

The workpiece material was used as Ti alloy Ti–6Al–4V in the experiment, and the workpiece size was 40 mm × 30 mm × 30 mm. Ti–6Al–4V is a type of $\alpha + \beta$ Ti alloy. This alloy is increasingly appreciated in aviation, spaceflight, navigation, and other industrial sectors due to its excellent unconventional mechanical properties (e.g., high hardness and strength, good thermal stability, strong corrosion resistance, outstanding antifatigue and antibreakage performance, and rich reserves). However, Ti alloy is difficult to process because of high temperature and stress during the processing [53]. The processing surface quality of products is difficult to be qualified, and the service life of tool will be shortened greatly. For these reasons, an experimental study on Ti–6Al–4V alloy processing must be performed. Tables 2 and 3 list the chemical composition and performance parameters of the workpiece, respectively.

The experiment used a machine-clamped milling tool, the tool pole model was 300R-C16-16-200-2T, the diameter (R) was 16 mm, the total length was 100 mm, the blade number was 2, and the material was quenched 42CrMo. The blade model was APMT1135, the tip angle was 85°, the blade rear angle was 11°, the thickness was 3.5 mm, the blade length was 11 mm, the maximum cutting depth was 9 mm, and the material was high-speed steel. According to the study of Junior

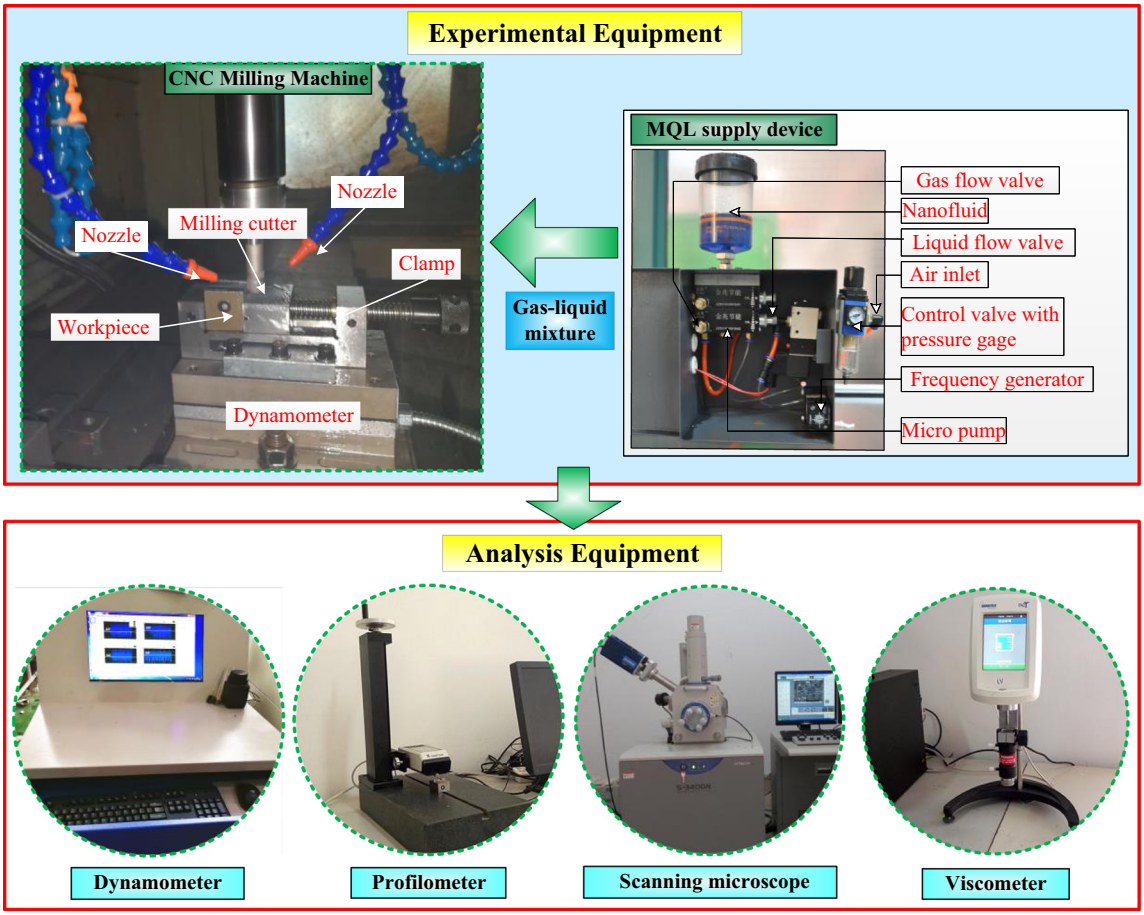

Fig. 1 Experimental and analysis equipment

[54], cottonseed oil can lower the cutting temperature, tool wear, and specific energy considerably. This oil owns the best cooling performance. In this experiment, cottonseed oil was used as the base oil of MQL, and six types of nanoparticles were added to prepare the nanofluids. Table 4 lists the physical properties of nanoparticles. Table 5 lists the physical, chemical, and mechanical properties of cottonseed oil. Table 6 lists the fatty acid composition of cottonseed oil.

2.3 Experimental scheme

In this experiment, cottonseed oil was used as the base oil of MQL, and six types of nanoparticles were added to prepare the nanofluids. Specifically, 1.5 wt% nanoparticles, cottonseed oil, and 0.3 wt% lauryl sodium sulfate (the dispersing agent) were mixed. The mixture was placed on a numerical control ultrasonic oscillator for 20 min of ultrasonic vibration.

Table 2 Chemical composition of Ti–6Al–4V

Workpiece material	Workpiece matrix	Alloying element (wt%)		Other elements (wt%)					
		Al	V	Fe	Si	C	N	H	O
Ti–6Al–4V	Ti	5.5–6.75	3.5–4.5	0.3	0.1	0.08	0.05	0.015	0.01

Table 3 Material performance parameter of Ti–6Al–4V

Modulus of elasticity (GPa)	Poisson's ratio	Tensile strength (MPa)	Yield strength (MPa)	Thermal conductivity (W/m °C)	Specific heat (J/kg °C)	Density (g/m^3)
114	0.342	950	880	7.955	526.3	4.42

Table 4 Performance parameters of different nanoparticles

Particle type	Al_2O_3	MoS_2	SiO_2	CNTs	SiC	Graphite
Particle size (nm)	70	70	70	70	70	70
Nanoparticle shape	Spherical	Layered	Spherical	Tubular	Hexahedral crystal	Layered
Moh's hardness	9	1–1.5	7	10	9.5	1–2

Table 5 Characteristics of cottonseed oils

Relative density (°C)	Refraction index (n D 40)	Acidity (g of oleic acid/100 g)	Density (g/m^3)	Flash point (°C)	Freezing point (°C)	Koettstorfer number	Viscosity (mPa s)
0.92 (20 °C) 0.93 (30 °C)	1.46–1.47	Max 0.3	0.919	324	5	191–199	70.4 (20 °C)

The vibration power of the numerical control ultrasonic oscillator was 60 W, and the vibration frequency was 2000 Hz. The processed mixture was used as the cutting fluid of NMQL. This concentration was selected on the basis of previous research. Wang et al. [55] reported that the optimal nanofluid concentration was 1.5 vol%. Figure 2 shows the configured nanofluid. Pure cottonseed oil was used as the control, and the control variable method was used. Table 7 lists different lubrication conditions.

In each experiment, only the type of lubricating fluid was changed. Uniform milling parameters were applied to analyze the effects of lubrication conditions on milling force and surface roughness (Table 8). Three repeated milling processes were conducted under different working conditions to reduce the contingency of the experiment, and the corresponding experimental data were collected.

3 Experimental results

3.1 Milling force

Milling force is an important physical quantity in the milling process, and its foundation is the process of machining deformation. Although Ti alloy material has strong chemical activity, small heat conductivity coefficient, and small elasticity modulus, it can be easily deformed and has poor rigidity, surface-resilient value, small deformation coefficient, high milling temperature, great milling force on unit area, and serious chilling phenomena. The flank surface of the tool presents serious friction, adhesion, and cementation wear, which influence the service life of the tool and workpiece surface quality. Therefore, studying milling force has significance to improving Ti alloy processing.

Milling forces were measured for three times under each working condition. The discontinuity of tool–workpiece contact causes dramatic changes in milling force because milling is a discontinuous cutting in nature. Figure 3 shows the variation law of cutting forces under different lubrication conditions. Milling force evidently presents a periodic variation law. For periodic peaks of milling force, $F_x > F_y > F_z$. The value of F_z is extremely small and slightly changes; thus, this value can be neglected. In high-speed milling, milling force is generally determined by the mean of peak (F_{max}). The mean of milling force peak $\left(\overline{F}_{max}\right)$ was used as a reference to discuss the effects of the seven working conditions on milling force.

$$\overline{F}_{max} = \frac{F_{max}}{N} = \frac{\sum_{i=1}^{N} F_{pi}}{N}, \quad (1)$$

where F_{pi} is the ith milling force peak in the collection signal of the milling force.

F_x, F_y, and F_z, which were collected by the measuring dynamometer and the calculated resultant milling forces, were integrated into Eq. (1) to obtain the corresponding milling force peaks (Fig. 4). Figure 4 shows that the maximum milling force was obtained by MQL ($F_x = 348$ N, $F_y = 202$ N). Regardless of which nanofluid type was milling, force was reduced to some extent compared with MQL. The milling force obtained by Al_2O_3 NMQL milling ($F_x = 312$ N, $F_y = 96$ N) was 10.34% and 52.48% lower than that of MQL, followed by that of SiO_2 NMQL ($F_x = 313$ N, $F_y = 107$ N). The worst one was that of graphite NMQL ($F_x = 330$ N, $F_y = 179$ N), which was 5.17% and 11.39% lower than that of

Table 6 Fatty acid of cottonseed oils (%)

Myristic acid	Palmitic acid	Stearic acid	Oleic acid	Linoleic acid	Linolenic acid	Others
0.6–1.0	21.4–26.4	2.1–3.3	14.7–21.7	46.7–58.2	ND–0.4	0.3–1.8

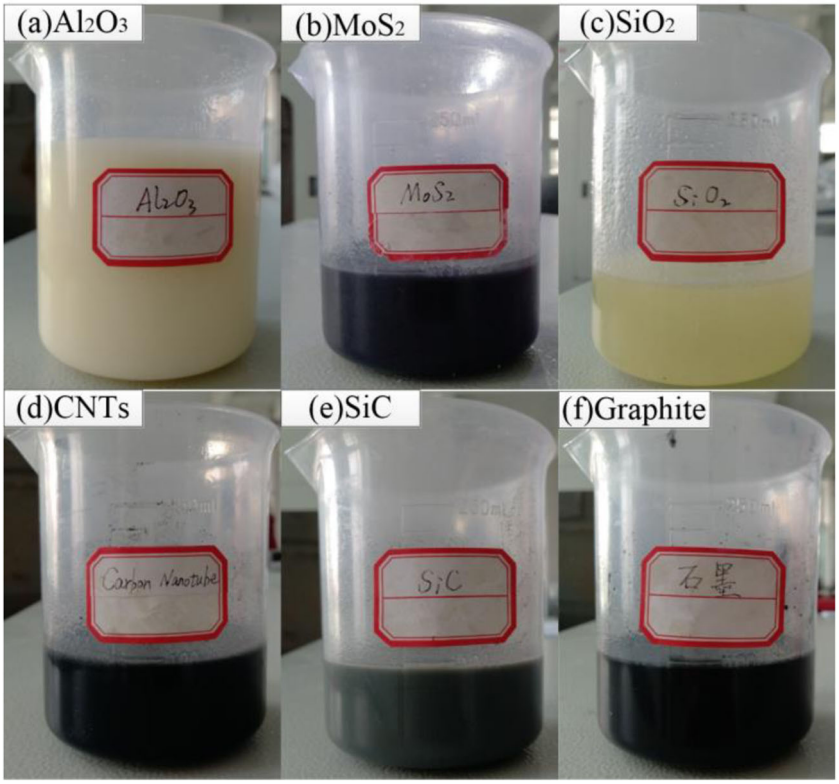

Fig. 2 Digital camera photos of different nanofluids

MQL. According to Eq. (2), under the condition of invariant other parameters, the reduction in cutting force would also lead to the decrease in specific energy in the machining process, and the specific energy reflected the amount of energy conversion in the milling process, which was an important index to measure the machining efficiency. Low specific energy reflected high processing efficiency under working conditions; therefore, the specific energy of Al_2O_3 NMQL milling was the smallest, and the corresponding processing was environmentally friendly and energy saving.

$$U = \frac{P}{Q_w} = \frac{F \cdot V}{\alpha_p \cdot \alpha_e \cdot V_f} = \frac{F \cdot R \cdot W_s}{\alpha_p \cdot \alpha_e \cdot V_f}, \quad (2)$$

where U represents the specific energy, P represents the total energy consumed, V represents the cutting speed, and Q_w represents the volume of material removed by tool.

Table 7 Different lubrication conditions

No.	Lubricating fluid
1	Al_2O_3 nanofluids
2	MoS_2 nanofluids
3	SiO_2 nanofluids
4	CNT nanofluids
5	SiC nanofluids
6	Graphite nanofluids
7	Pure cottonseed oil

3.2 Friction coefficient (μ)

The value of friction coefficient reflects the lubrication effect of a tool–workpiece interface. A small friction coefficient results in an improved lubrication effect. The cutting force measurement was obtained in the workpiece coordinate system; however, the calculation of friction coefficient (μ) required radial cutting force (F_r) and tangential cutting force (F_t) under the cutting coordinate system. The directional cutting force (F_r, F_t) could be calculated by experimental cutting force (F_x, F_y) by using the following transformation method: In the end milling, friction coefficient was the ratio of F_r to F_t. The calculation formula is [56]

$$\begin{bmatrix} F_r \\ F_t \end{bmatrix} = \begin{bmatrix} \sin(\gamma - \omega_s \cdot t) & -\cos(\gamma - \omega_s \cdot t) \\ \cos(\gamma - \omega_s \cdot t) & \sin(\gamma - \omega_s \cdot t) \end{bmatrix} \begin{bmatrix} F_x \\ F_y \end{bmatrix}, \quad (3)$$

$$\mu = \frac{F_r}{F_t}, \quad (4)$$

where γ is the cut in angle and t is the processing time (ms).

Figure 5 shows that the highest friction coefficient was obtained by MQL (0.79). The lowest friction coefficient was obtained by Al_2O_3 NMQL (0.413), which was 47.7% lower than that of MQL. The friction coefficient of SiO_2 NMQL was second (0.426), which was 46.1% lower than that of MQL. The highest friction coefficient was

Table 8 Experimental parameters

Milling parameters	Numerical value
Milling method	End milling
Rotation rate, W_s (r/min)	1200
Feed rate, V_f (mm/min)	500
Back engagement of the cutting edge, a_p (mm)	0.25
Working engagement of the cutting edge, a_e (mm)	10
MQL flow rate (ml/h)	50
MQL nozzle distance (mm)	30
Angle of the nozzle and the tool feeding direction, α (°)	50
Angle of nozzle and horizontal direction, β (°)	30
MQL air pressure (MPa)	0.5

obtained by graphite nanofluid (0.633) as NMQL, followed by that of SiC nanofluid (0.578). If the friction coefficient was higher than 0.5, then the adhesive friction and flow only occurred in the workpiece but not on the tool–workpiece interface. The secondary shearing effect indicates that deformed debris will be thickened, accompanied with reduction in cutting ratio and shearing angle and growth of the shearing length. As a result, the force and power to remove debris will be increased remarkably.

3.3 Surface roughness

Surface roughness is an important parameter for workpiece surface quality evaluation and determines surface smoothness. Surface roughness refers to a small space of the processed surface and the size features of micro-geometry with tiny peak valley and unevenness. Low surface roughness reflects high surface smoothness. Surface roughness can influence fatigue strength, contact stiffness, and corrosion resistance of workpiece and substantially improve cooperation. Moreover, surface roughness influences the service life and reliability of machinery products. A poor surface quality will deteriorate workpiece performance, and the workpiece will fail before the expected life.

R_a is the arithmetic mean of absolute deflection distance (Z) between the profile points and baseline in one sampling length (L). A high R_a indicates a large absolute value of profile deflection distance. R_a was calculated using Eq. (5), where y (x) is the vertical coordinate of the profile curve.

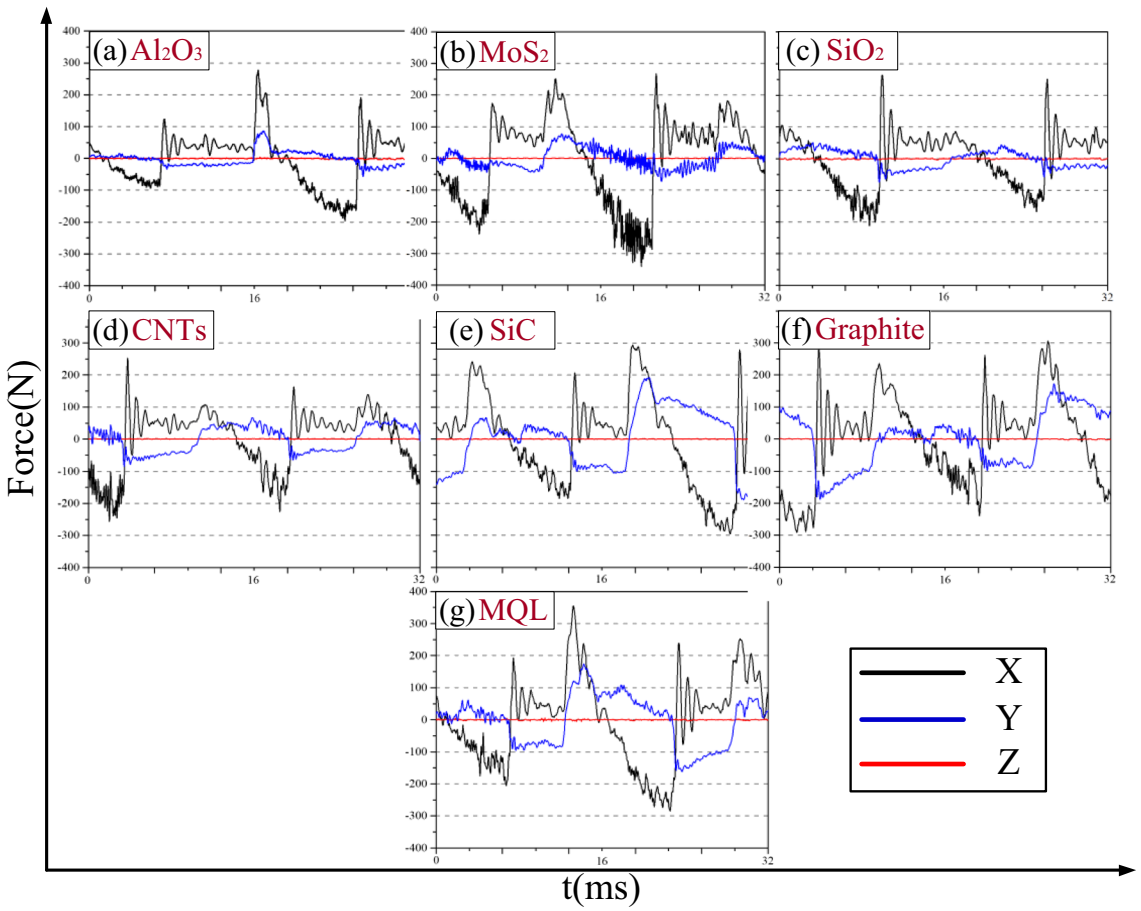

Fig. 3 Original data schematic of force

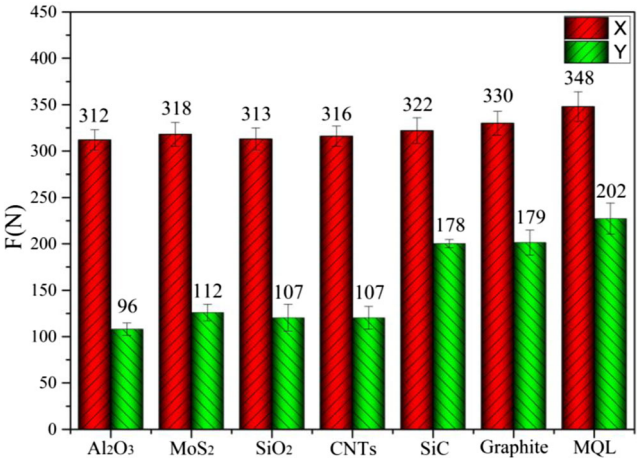

Fig. 4 Schematic of component force

$$R_\alpha = \frac{1}{L}\int_0^L |y(x)||d_x|, \tag{5}$$

RS_m is the mean of profile irregularity distance in sampling length L. Profile irregularity distance refers to the length of profile peak and the adjacent profile valley on the median. This parameter can be calculated from the following equation:

$$RS_m = \frac{1}{N}\sum_{i=1}^{n} S_i, \tag{6}$$

where N is the number of profile peaks at the mean line.

R_{mr} is the roughness profile support length ratio, which is the ratio of contour support length to sampling length. The length of the contour support is the sum of the length of each section in the sampling length (ln), which is parallel to the center line and is separated from the contour peak line c by the truncation of the line and the contour. The R_{mr} curve reflects the relationship between the support length ratio of roughness profile and the horizontal cross-section height c. R_{mr} was calculated by

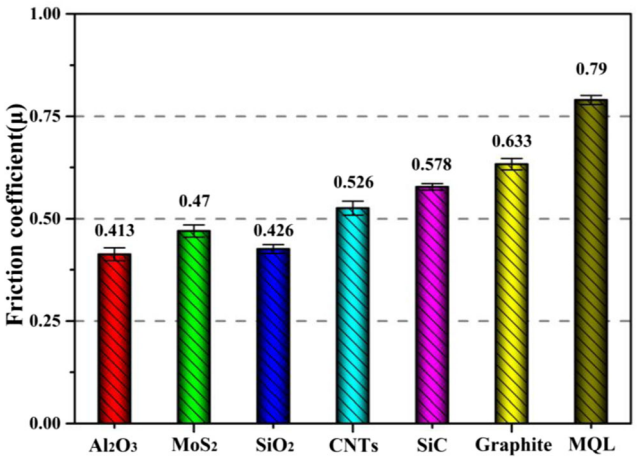

Fig. 5 Friction coefficient under different working conditions

$$R_{mr} = \mathrm{M}l(c)/l\mathrm{n}. \tag{7}$$

Five points on workpiece surface acquired under each working condition were selected to measure surface roughness, thereby obtaining seven groups of correlated roughness values (Fig. 6). R_a, RS_m, and their standard deviation were selected as the evaluation parameters of roughness. Surface roughness value (R_a) was gained under different lubrication conditions, and its standard deviation was measured using a roughness-measuring device (Fig. 7). Figure 8 shows RS_m and its standard deviation.

Figure 7 presents that the surface roughness (R_a) under MQL processing was the highest (1.596 μm), which indicated the roughest surface. The workpiece surface roughness (R_a) under NMQL processing was lower than that under MQL processing to different extents. The lowest surface roughness was gained under SiO_2 NMQL processing ($R_a = 0.594$ μm), which was 62.78% lower than that under MQL processing. The surface roughness under Al_2O_3 NMQL ($R_a = 0.633$ μm) processing was the second lowest, which was 60.34% lower than that under MQL processing. The values of R_a under the CNTs and graphite NMQL were 0.867 and 0.906 μm, respectively, which indicated poor workpiece surface quality. SiC NMQL milling showed the poorest surface quality ($R_a =$ 0.94 μm). The standard deviation of R_a under Al_2O_3, SiO_2, and MoS_2 NMQL was small, which reflected the small dispersion degree of R_a at different points of the workpiece to the mean value. In other words, the entire workpiece surface showed relatively high accuracy.

The RS_m value on the surface of the machined workpiece reflects the scratch diameter in the cutting process. Large scratch diameters can reduce the surface quality of the workpiece. Figure 8 shows that RS_m under MQL processing was the highest (0.399 mm), which reflected the maximum average width of the surface profile scratches caused by MQL milling. The lowest RS_m was observed under Al_2O_3 NMQL (0.095 mm), which showed the minimum average width of scratches and the best workpiece surface quality. RS_m under SiO_2 NMQL (0.11 mm) was the second lowest. RS_m under SiO_2 NMQL was higher than that under Al_2O_3, which was related to the weaker milling force and tool vibration under Al_2O_3 NMQL. The values of RS_m under CNTs and SiC NMQL were 0.193 and 0.208 mm, respectively, which indicated poor lubrication effect. Graphite NMQL milling showed the poorest lubrication performance ($RS_m = 0.295$), manifested by large scratches on the workpiece surface. The standard deviation of RS_m under CNT NMQL, graphite NMQL, and MQL was relatively high, which revealed the high dispersion degree of RS_m to the mean. The difference among transverse components of surface roughness at different points of the workpiece surface increased due to the great tool vibrations caused by the strong milling force.

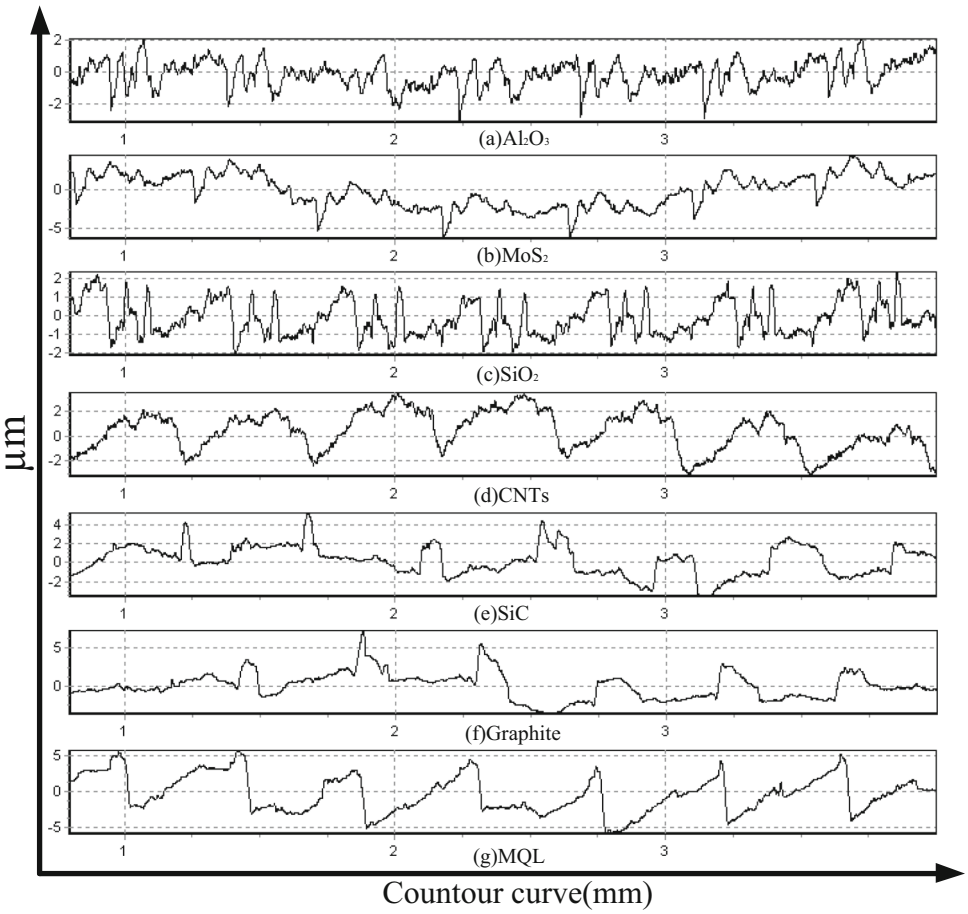

Fig. 6 Typical signal image of surface roughness measurement

The microstructures of workpiece surface under similar R_a and RS_m differed considerably. The surface characteristics were different. Therefore, surface quality must be evaluated, and it is inadequate to reflect all features of surface roughness by R_a and RS_m. The shape feature parameters of microscopic irregularity were represented by R_{mr} curve. This curve can reflect the wear resistance of the workpiece surface. Difference in surface profiles leads to great changes in actual contact area between the lubricating oil and workpiece, thereby resulting in different wear resistances of processed surfaces. Among the longitudinal evaluation parameters (R_a) and transverse evaluation parameters (RS_m) gained under the above seven working conditions, SiO_2 gained the lowest surface roughness (R_a) and Al_2O_3 gained the lowest RS_m. Therefore, the profile support length ratio of workpiece surface under SiO_2 and Al_2O_3 NMQL was used to analyze the

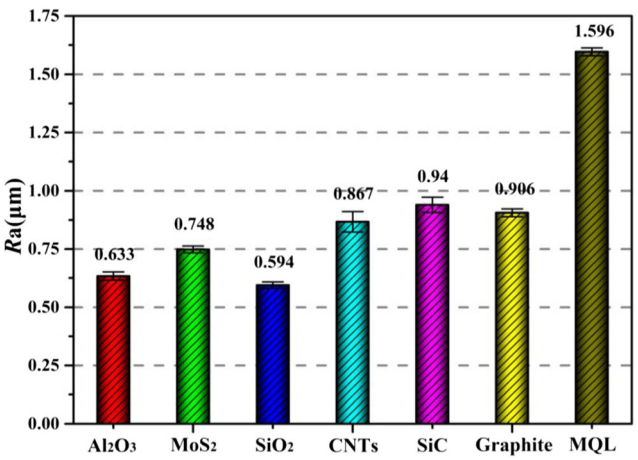

Fig. 7 R_a under different working conditions

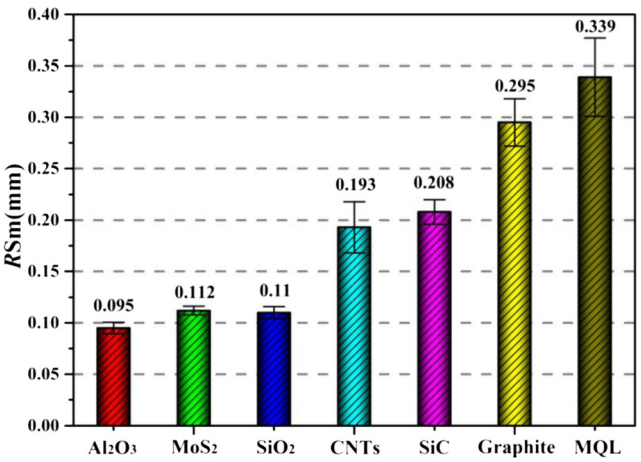

Fig. 8 RS_m under different working conditions

functional characteristics of the workpiece surface. According to the studies of Zhang [46] and Liu [57], the profile support length ratio (Mr_1) was determined for one section line that separated profile peak from the roughness core profile. The profile support length ratio (Mr_2) was determined for one section line that separated the profile valley from the roughness core profile.

Figure 9 shows the R_{mr} curve. Mr_1 under the SiO_2 NMQL working condition was close to the left, which indicated few heaves on the workpiece surface. On the contrary, Mr_1 under the Al_2O_3 NMQL was close to the right, which implied abundant heaves on workpiece surfaces and a relatively poor surface quality. R_{mr} is the ratio between profile support length and sampling length, and low Mr_2 implies a large profile valley. Mr_2 under SiO_2 NMQL was close to the left, which reflected a large profile valley on the working surface. Abundant deep furrows were observed on the processed workpiece surface. However, large profile valleys were conducive to storing oils, thereby improving the lubrication performance effectively. On the contrary, few profile valleys existed on the processed workpiece surface under Al_2O_3 NMQL; consequently, the oil storage capacity was low. In brief, the workpiece surface under SiO_2 NMQL was the best.

3.4 Debris surface topography

In the process of metal cutting, especially in the process of high-speed cutting, the shape of debris is important, and its change affects the surface quality of the workpiece and the service life of the tool [58]. The formation process of debris is the essence and foundation of physical and chemical phenomena in cutting process, such as cutting force and temperature.

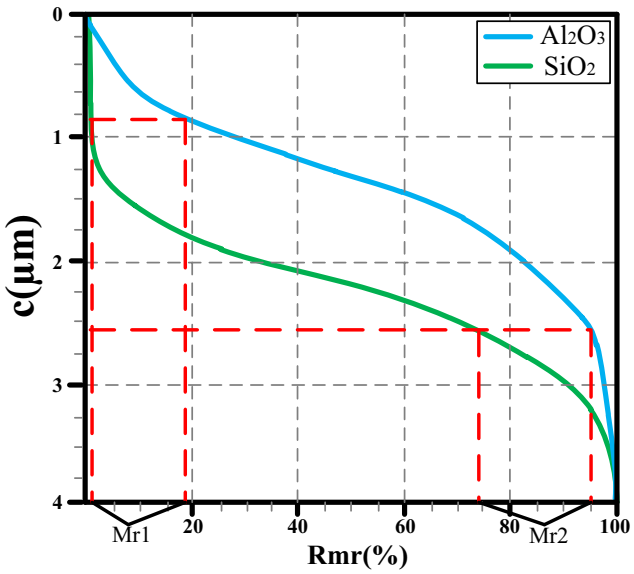

Fig. 9 Profile supporting length rate curve

Therefore, the morphological characteristics of debris must be studied to understand the mechanism of high-speed cutting and improve machining efficiency [59]. Debris, which was formed under different lubrication conditions, was collected. A qualitative analysis of lubrication performance under different conditions was performed by observing the morphology and surface characteristics of debris. SEM was used to analyze the shape of debris and the surface morphology on the back of debris. Figure 10 shows SEM images of milling debris under different lubrication conditions. Figure 11 shows the schematic of debris formation in different shapes.

As shown in Fig. 10, the back of debris was the contact surface between the rake face of the tool and debris. The back of debris was smooth and bright. In the grinding process, the back of debris slid along the rake face of the tool and was extruded and cut by the rake surface. This contact surface experienced high contact stress and shear stress, and obvious scratches along the debris outflow were developed. The scratches were regular straight line. Scratches on the back of debris were caused by the cohesive action between Ti alloy and tool. At flowing of debris, hard particles on the tool surface might scratch the Ti alloy and generate scratches on the contact surface (Fig. 11). High temperature in the processing could intensify the production of scratches [60]. The scratching effect of hard particles can easily cause mechanical wear of the tool [2]. Hence, thick scratches led to poor processing conditions. The free surface, that is, the noncontact surface between debris and the tool, presented a hairy layer and uneven surface. Tremendous dense strips were caused by shear plastic deformation. The processed workpiece surface was composed of multiple irregular hairy layered shearing surfaces. Different shearing surfaces had different shapes and sizes. Local dislocation occurred among different sharing surfaces. The debris was presented in a strip.

The deformation of the debris in Fig. 10a–e was restricted by the angle of cutting edge. The debris was discharged naturally and was in helical curling shape. The morphological features of the debris remained basically the same using different types of nanoparticles. However, the screw pitch of helical curling debris varied, thereby causing changes in the length of debris after curling. The screw pitch was 27.2 mm in Fig. 10a and 29.5 mm in Fig. 10b. The debris in Fig. 10a was the slenderest and had the minimum screw pitch. Under working conditions in Figs. 10c, d, the stress and strain on the debris increased, which induced the gradual increase in the screw pitch of the debris. Under the working conditions in Fig. 10f, g, the debris was C shaped. This feature was due to that the cutting force per unit area of the debris increased with the increase in milling force, which could increase the curling degree and break of the debris. One side of the debris exhibited relatively regular arcs, and the other side had extremely irregular deckle edges, accompanied with breakages.

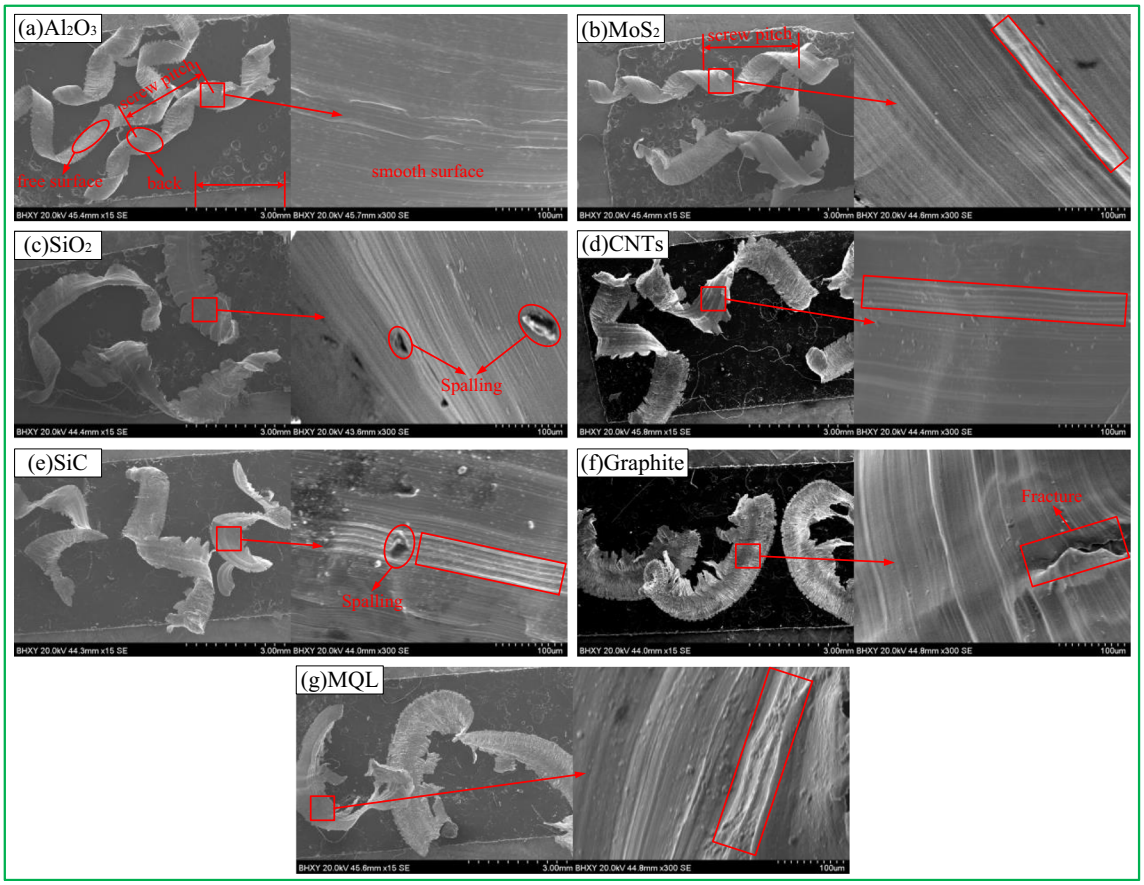

Fig. 10 SEM images of debris surfaces under different working conditions

The back of debris contacted with the rake face of the tool. The tool performance in the process could be analyzed from the back of debris. The back of debris was amplified by SEM. Figure 10g, f shows that the milling surface quality under MQL and graphite nanoparticle grinding was relatively poor. The surface was rough and had many irregular scratches. Plasticity accumulations were observed on the milling surface under MQL, accompanied with many scratches on the tool. The scratches were very wide, and the back of debris was rough, which indicated the serious scratches of hard points on the rake face of the tool to the back of debris under MQL conditions. The workpiece surface after graphite nanofluid-based milling reflected that debris had experienced great shear plastic deformation. Cracks would scratch the rake face and cutting edge of the tool, thereby resulting in high-frequency vibrations of the cutting system and influencing the workpiece surface quality. Under the two working conditions, strong milling force and high temperature not only increased the

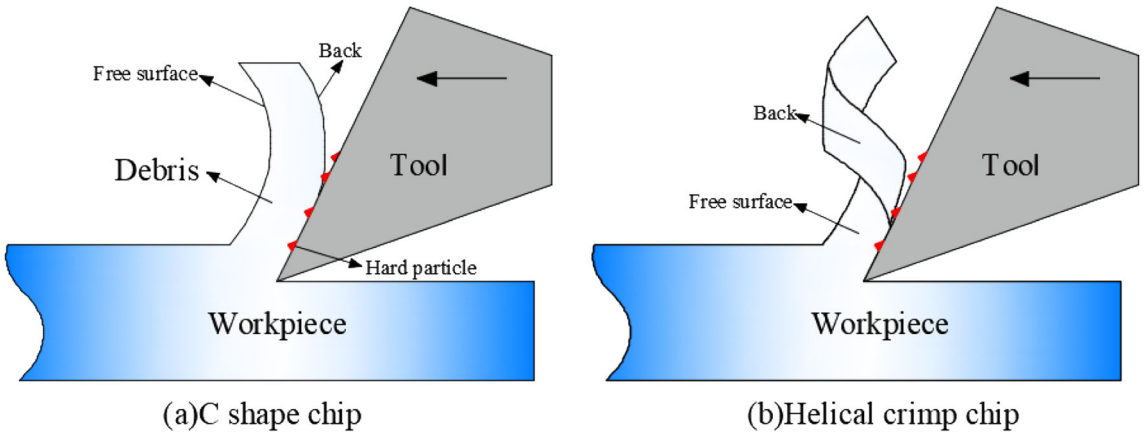

Fig. 11 Schematic of different shapes

strain rate of materials but also strengthened the thermal softening effect. The interaction of the two effects caused the material fragility to change. A small disturbance in the milling process would cause instant release of accumulated cutting heats on the shear surfaces, which was conducive to shear slip. Therefore, the deformation of debris was intensified, and the lubrication performance was deteriorated.

Scratches on the back of debris were relieved to some extent under SiO_2 and SiC NMQL. However, this phenomenon was manifested in the reduction in scratch width rather than in quantity. The back of debris had poor smoothness and evident peeling offs. Although the workpiece surface was relatively rough, it was improved remarkably compared with that under MQL milling.

The debris gained from MoS_2 and CNT NMQL had a relatively smooth surface without evident peeling offs. The debris under MoS_2 NMQL was more regular than that under CNT NMQL, but scratches on the debris under these working conditions were more obvious than those under Al_2O_3 NMQL. The debris under Al_2O_3 NMQL had the best morphology. They were thinner and longer than those under other working conditions. The workpiece surface was also smoother, without evident scratches of the tool. The workpiece surface morphology was improved substantially, and metal deformation in the cutting layer became more uniform. The free surface of debris was relatively smooth, and the thickness of debris remained basically the same. The contact between the tool and debris changed from conventional local fitting to close fitting, and the frictional scratches on the bottom surface of debris deceased gradually. The bottom surface of debris became increasingly smooth. These results demonstrated that different NMQL techniques could improve the processing morphology of debris to some extent, thereby improving the workpiece surface quality and service life of the tool.

3.5 SEM and EDS of workpiece surface topography

SEM and energy-dispersive spectrometer (EDS) are two common analytical devices in the field of modern material analysis. They are basically combined to observe the surface morphology of a sample and to analyze microregion composition. The surface quality of workpiece was analyzed by SEM, and the composition of surface elements was analyzed by EDS.

Figure 12 shows that the workpiece surface developed corrugated textures, which were the surface morphology caused by a relative movement between the tool and the workpiece. Corrugated textures reflected the motion trajectory of the cutting edge. The shape of the cutting edge was duplicated on the workpiece surface. The displacement of each ridge with a uniform interval along the feeding direction was equivalent to feed engagement in milling parameters.

The workpiece surface developed the thickest irregular furrows under MQL milling. Two furrows were very close due to the tool wearing, which explained the highest surface roughness under this working condition. The workpiece surface under SiC and graphite NMQL showed thicker furrowers than those under other NMQL milling processes, which reflected that hard points on the tool surface plowed the workpiece surface most seriously. The rough grooves on the wearing surface of tool were copied onto the workpiece surface. Strong extraction and friction behavior occurred on the contact surface between the cutting edge and workpiece (Fig. 12e, f). The workpiece surface developed many scratches under CNT NMQL (Fig. 12d), which indicated the high quantity of hard points on the tool surface. These hard points plowed the workpiece surface greatly, and the tool suffered serious wearing. The protuberant ridges were not a line but became a furrow band composed of many small wearing-induced heaves and grooves. Furrows could not only influence the processed surface roughness but also act on the tool surface in return, which caused the tool surface to generate additional grooves that intensified tool wearing. Hence, a vicious circle was formed. The workpiece surface under MoS_2 NMQL developed distinct furrows (Fig. 12b), whereas the workpiece surface under Al_2O_3 NMQL showed a great quantity of scratches (Fig. 12a). On the contrary, the workpiece surface under SiO_2 NMQL had shallow scratches and the lowest surface roughness (Fig. 12c).

Lubrication film plays an important role in lubrication during cutting. Nanoparticles deposited on the workpiece surface can reduce shear stress and thus decrease friction and wearing. EDS was used on the elements of workpiece surface to evaluate the formation of the nanolubrication film on the workpiece surface. Figure 12 shows that the Al content in the workpiece surface under Al_2O_3 NMQL was 3.93% higher than that under MQL milling. Therefore, the Al_2O_3 NMQL deposited on the workpiece surface in a large quantity during the processing and the Al_2O_3 nanoparticles were conducive to forming lubrication film [61]. On the workpiece surface, Al formed the element deposition for the formation of lubrication film, thereby increasing the lubrication performance. On the contrary, the S content on the workpiece surface under MoS_2 NMQL was relatively low. The Si contents on the workpiece under SiO_2 and SiC NMQL were 0.31% and 0.09%, respectively. These results demonstrated that nanoparticles could not deposit onto workpiece surfaces stably under these working conditions. SiO_2 NMQL milling achieved the best workpiece surface quality, which indicated a better lubrication performance under SiO_2 NMQL. However, the formed lubrication film could not adhere onto the workpiece surface stably. The C contents on the workpiece surface under CNTs and graphite NMQL reached 4.72% and 5.31%, respectively, but the workpiece surface quality was poor.

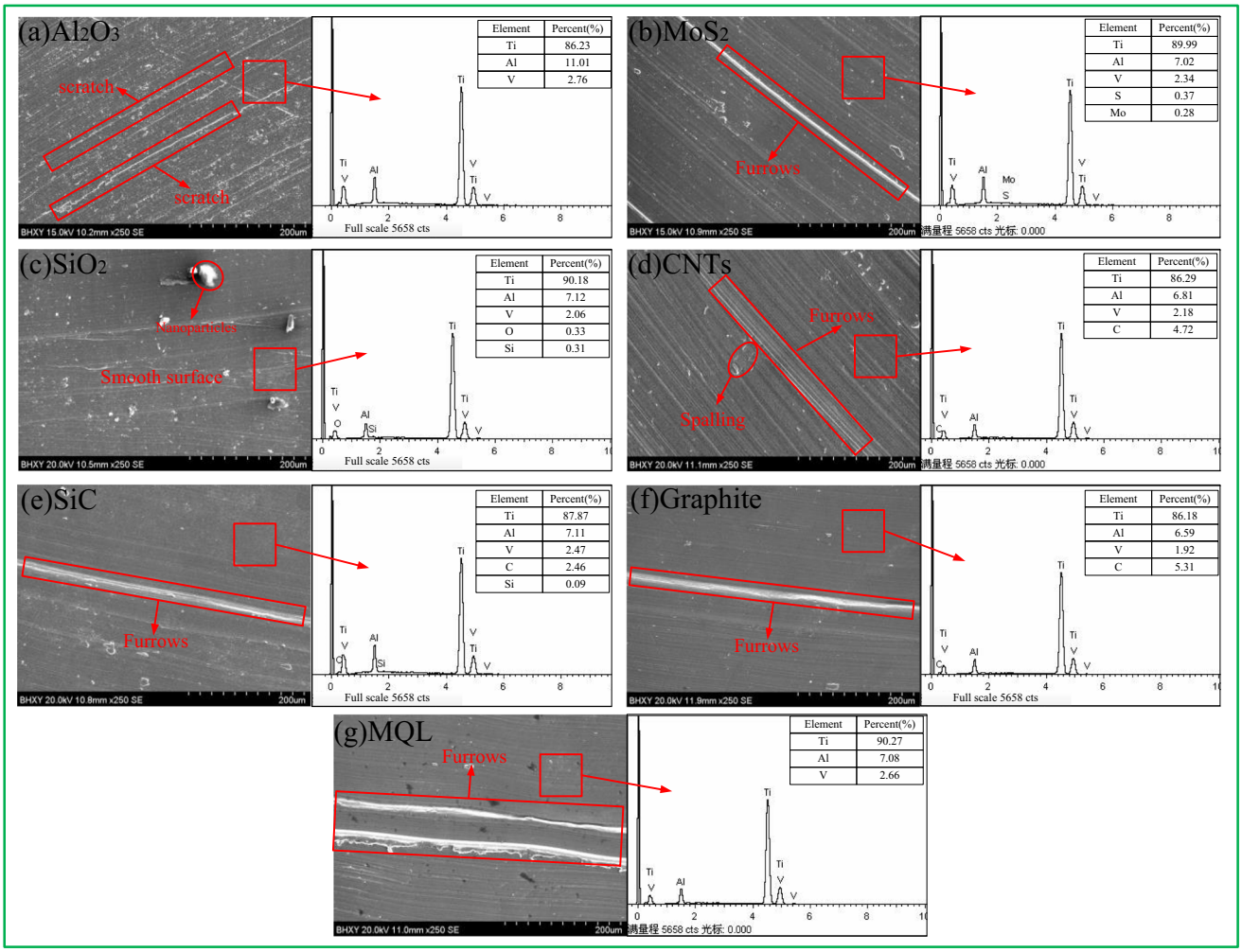

Fig. 12 SEM and EDS images of workpiece surfaces under different working conditions

4 Analysis and discussion

4.1 Analysis of the physicochemical properties of nanoparticles

The presence of nanoparticles can considerably reduce the contact of tool and workpiece. During NMQL, nanofluids were carried by high-pressure gas and formed extremely small fog drops in nozzles. Nanoparticles with strong polarity adhered onto the tool and workpiece surface through deposition or adsorption, which formed a piece of lubrication film on the friction surface (Fig. 13). This lubrication film could prevent direct contact between the tool and workpiece surface. Nanoparticles were embedded into the lubrication film, and nanofluids penetrated the cutting zone under the assistance of high pressure for antifriction and antiwear. This characteristic could improve the lubrication effect in the cutting zone remarkably.

Surface atoms of nanoparticles can easily combine with polar atoms in cottonseed oil, which causes nanofluids to produce high surface energies and adsorb onto tool and workpiece surface strongly. Therefore, the lubrication performance is improved. Nanoparticles can also develop “the ball effect” and “filling effect” in the processing [62]. The ball effect

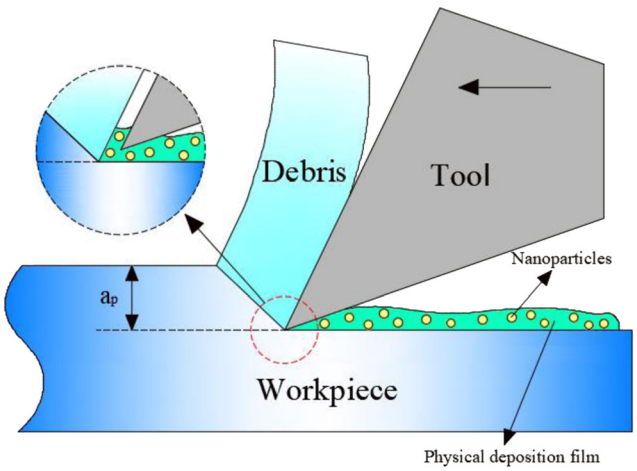

Fig. 13 Schematic of the physical deposition of nanoparticles

indicates that spherical or approximately spherical nanoparticles can serve as rolling bearings on the friction surface with good smoothness and turn the sliding friction into rolling friction, thereby reducing the friction coefficient. Excellent antifriction performance is developed [63–65]. "The filling effect" indicates that nanoparticle will deposit into the developed cracks, scratches, or grooves on workpiece surface to repair the workpiece surface to a certain extent. This effect reduces the wear and friction coefficient of the workpiece and improves the lubrication performance in the processing [66]. Nanoparticles can polish the workpiece surface. The roughness of the friction pair decreases and the contact area increases after the polishing, and this condition further causes reduction in the friction coefficient. The pressure stress on the contact surface decreases, which is beneficial to increasing the bearing capacity of the lubricating oil. In the milling process, although the lubrication film will be eliminated as the milling process continues, nanoparticles can be easily adsorbed onto the workpiece surface because of the secondary penetration of nanofluids and secondary formation of the lubrication film. Broken lubrication films by cutting can be supplemented and updated rapidly through the subsequent adsorption [67]. The physicochemical properties of nanoparticles are important factors that influence the lubrication performance of lubrication films. Figure 14 shows the molecular structure of different nanoparticles.

Figure 14a shows the molecular structure of Al_2O_3. O atoms are in the tight hexagonal arrangement, and Al distributes symmetrically in the octahedral coordination center surrounded by O atoms. Strong chemical bond polarity exists between Al and O, and great lattice energies occur. With these structural features, Al_2O_3 nanoparticles possess high melting point and strength and good chemical stability. The spherical structure [68] provides a good lubrication performance and can offer some mechanical polishing effects on the workpiece surface, which are conducive to forming a good workpiece surface morphology. With a strong adsorption performance, substantial lubricating oil can be adhered onto the workpiece surface. Base oil enters the cutting zone to repair the oil film and increase the coverage area of the oil film in the cutting zone, thereby developing a satisfying lubrication performance. Al_2O_3 nanoparticles show excellent antifriction in the processing and serve as the support on the tool–workpiece interface due to their high hardness. They narrow the actual contact area of the friction pair, decrease the frictional force, and inhibit the workpiece surface furrows by the tool. The

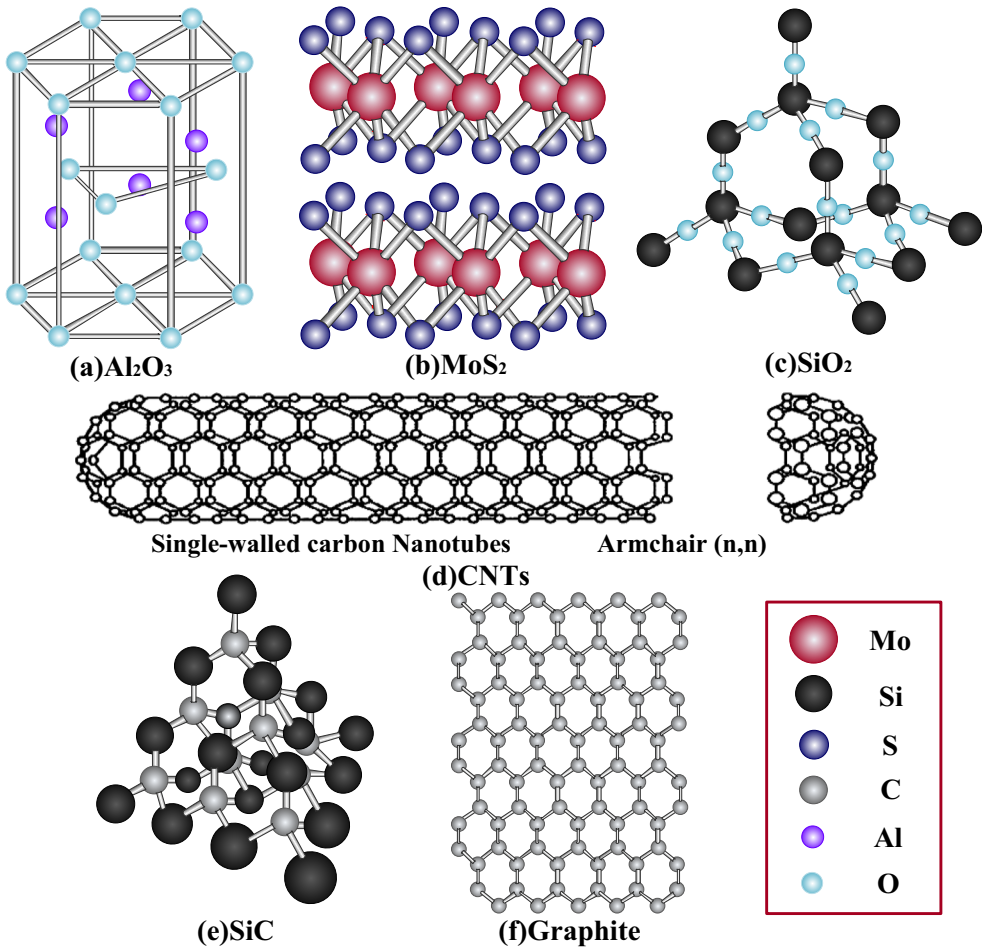

Fig. 14 Schematic of the molecular structures of different nanoparticles. **a** Al_2O_3. **b** MoS_2. **c** SiO_2. **d** CNTs. **e** SiC. **g** Graphite

high-temperature resistance of Al_2O_3 nanoparticles can strengthen the lubrication film and improve the high-temperature resistance and antifriction of the lubrication film.

MoS_2 nanoparticles are ellipsoid and connected by stratified structures. The good lubrication performance of MoS_2 nanoparticles is determined by the molecular structures (Fig. 14b). Each molecular layer of MoS_2 consists of three atom layers. The upper and bottom layers are S atom layers, and the middle is the Mo atom layer. Each Mo atom is surrounded by six S atoms. The research of Zhang [69] and Kalin [70] demonstrated that a plane with low shear force is produced by the strong binding force between S and Mo atoms in each molecular layer and the weak binding force between S and Mo atoms in each molecule. This molecular layer can be easily broken by a small shear force among molecules, thereby forming tremendous glide planes. As a result, the direct contact of friction pair surfaces in relative friction states is changed into relative sliding among MoS_2 molecular layers. The MoS_2 physical films that fall off in the sliding process can be supplemented and updated rapidly by subsequent adsorption to maintain such sliding behavior. Hence, a good lubrication performance can be offered.

Figure 14c shows the molecular structure of SiO_2. Each Si atom is surrounded by four O atoms, which form a tetrahedral structure. This structure determines the high strength of SiO_2 nanoparticles and can cooperate with the spherical structures of SiO_2 nanoparticles to polish the workpiece surface. SiO_2 possesses high surface energy and surface activity and can be easily deposited on workpiece surface to form the lubrication film [71]. SiO_2 nanoparticles can react with base components on the workpiece surface or subsurface to form a solid solution. This solid solution can develop a layer of ceramic-alike nanofilm, which is called "the third body." This nanofilm differs considerably from common oil films. The ceramic-alike nanofilm is superior to other oil films in terms of tenacity and compressive strength [72]. The nanofilm can reduce the friction on the tool–workpiece interface remarkably. SiO_2 nanoparticles distributes uniformly in the lubrication film due to the strong diffusion capacity and self-diffusion capacity, which narrows the effective contact area of adhesion effect. Elasticity is enhanced in a certain loading range with the increase in the gap between tool and workpiece surface due to the high porosity of spherical SiO_2 nanoparticles, and a good workpiece surface morphology is obtained.

The molecular structure of CNTs can be simplified into a coaxial circular tube with multiple layers composed of C atoms in hexagonal arrangement (Fig. 14d). The high strength and hardness of CNTs strengthen the lubrication film and decrease sliding friction coefficient. However, the oil film is not complete, which is related to the geometric features of CNTs (e.g., circular shape and easy twining) [73, 74]. Large-scaled twining accumulation is formed on the friction pair surface rather than the ball effect similar to spherical nanoparticles. EDS analysis demonstrates a high C content on the workpiece surface, but the formed lubrication film has limited lubrication performance. These results explain the poor workpiece surface quality under CNT NMQL.

SiC, or known as the carborundum, is the compound formed by C and Si atoms through covalent bonds. This compound possesses outstanding chemical and thermal stabilities and excellent mechanical and thermal conductivities (83.6 W/m K). Adding SiC nanoparticles to the base oil increases the heat conductivity coefficient of the base oil due to the high heat conductivity coefficient, thereby enhancing the heat exchange of nanofluid. This addition strengthens the lubrication performance of nanofluid to some extent. The crystal structure of S is formed by alternative bedded deposition of C and Si atoms (Fig. 14e). Although this compound has some self-lubrication performance, it belongs to hard material with Moh's hardness of 9.5 and a multiangular physical property. Therefore, adding SiC nanoparticles fails to improve the lubrication performance of nanofluid considerably.

Graphite nanoparticles, typical stratified structures, have layered arrangement of C atoms. Each C atom is connected with adjacent C atoms in the equivalent interval. C atoms in one layer are in hexagonal ring arrangement. The hexagonal C rings in the adjacent upper and lower layers displace mutually along the parallel surface and then form the stratified structure through re-superposition. Different orientations and distances of displacement determine the diversified polymorphic structures (Fig. 14f). Some studies have indicated that graphite nanoparticles present antifriction and antiwear. However, they are inferior to other nanoparticles due to the stratified structure and high strength. Graphite cannot form "bearing-alike effect" and develop a sliding layer similar to MoS_2. Therefore, the lubrication performance of graphite nanoparticles is poor.

4.2 Viscosity analysis

Viscosity is a method to measure the flow resistance of fluid. This method is the variable exchange formed by the irregular relative movement of molecules and the adhesive force among adjacent molecules. Viscosity is also equal to shear force/shearing rate. The viscosity of lubricating oil is an influencing factor of lubrication performance. Adding nanoparticles to the base oil can increase the viscosity of lubricating oil. During workpiece processing, the relative movement between the tool and workpiece will induce shear forces to the lubricating oil. As a result, internal friction force is developed among the internal fluid layers of the lubricating oil, which will influence the internal friction force. Such a property is defined as viscosity. Viscosity can affect the formation of oil film to some

extent. Lubricant with small viscosity is difficult to form sufficiently thick oil films on a high-temperature frictional surface, and the formed oil film can be easily damaged by external loads due to the small bearing capacity, thereby resulting in the poor lubrication performance of friction pairs and high friction coefficient. The relationship between the viscosity of nanofluid and the viscosity of base oil can be disclosed from the Einstein's law of viscosity in Eq. (8). Figure 15 shows the viscosity–temperature curves of different nanofluids.

$$\frac{\mu_{\mathrm{n}}}{\mu_{\mathrm{bf}}} = 1 + 2.5\varphi, \tag{8}$$

where μ_{n} is the viscosity of the nanofluid, μ_{bf} is the viscosity of the base fluid, and φ is the nanoparticle volume fraction.

On this basis, Batchelor considered the Brownian motion of nanoparticles and proposed the following formula:

$$\mu_{\mathrm{n}} = \left(1 + 2.5\varphi + 6.5\varphi^2\right)\mu_{\mathrm{bf}}. \tag{9}$$

Figure 15 shows the negative correlation between the viscosity of nanofluid and temperature. This negative correlation is due to that the viscosity of fluid is a collaborative result of molecular attractions and momentum transfer. The change in the molecular energy of nanoscale fluid can be caused by the change in temperature. For liquid molecules, the average speed of irregular movement is low. The molecular interaction takes the dominant role in viscosity. Molecular distance increases with the temperature rise, which weakens the molecular interaction and thus reduces the viscosity. The viscosity of different nanoparticles is different mainly because of the interaction of particles, the Brownian motion effect, and the interaction between particles and base oil. The molecular structure of tetrahedron of SiO_2 nanoparticles leads to great interaction among molecules, and the Brownian motion is inactive. Consequently, the viscosity of SiO_2 nanoparticles is high under the condition of the same volume fraction and base oil. The different thermal movements of molecules among different nanoparticles lead to the difference in the viscosity of different nanofluids with temperature.

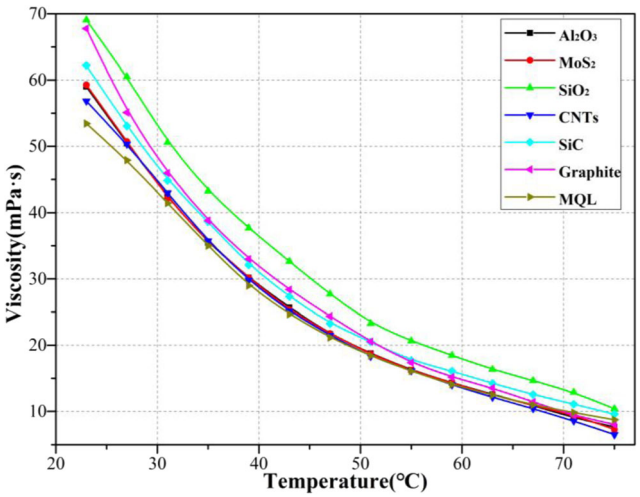

Fig. 15 Viscosity–temperature curves of different nanofluids

SiO_2 nanofluid has the highest viscosity, which reaches 69.06 mPa s under room temperature. The lubrication performance of lubricating oil is improved with the increase in viscosity, but the lubrication performance declines after reaching a certain numerical value [75]. Comparison of surface roughness (R_{a}, RS_{m}) and workpiece microstructure indicates that SiO_2 NMQL achieves the best workpiece surface quality. This result demonstrates that viscosity is insufficiently high to stop liquid flow. In this case, high viscosity is accompanied with strong colloidal force, Brownian movement, and viscosity force among molecules. High viscosity is conducive to stopping liquid flow, forming oil film, and increasing the thickness and strength of the lubrication film [76]. Lubricating oil with high viscosity can stay in the milling zone for a long time and prolongs the lubrication time between the tool and workpiece. This feature can improve the lubrication performance and prevent the fast wearing of the tool effectively.

The viscosity of graphite and SiC nanofluid is only next to that of SiO_2 nanofluid. However, graphite and SiC fail to achieve a satisfying workpiece surface quality because the physicochemical properties of nanoparticles are vital to the lubrication performance. The analysis of the physicochemical properties of graphite and SiC presents that increasing nanofluid viscosity can deteriorate the lubrication performance. Pure cottonseed oil and CNT nanofluid have small viscosity, which results in the thinning of oil films. If the oil film between the tool and workpiece surface is too thin, then it will break in the processing and local dry friction will be formed, which will further intensify the wearing [77]. This finding, along with the experimental results, shows that the workpiece surface quality under graphite and SiC NMQL is poor, which indicates the positive correlation between viscosity and lubrication performance.

The viscosity–temperature curves of Al_2O_3 and MoS_2 nanofluid overlap. However, the workpiece surface quality under Al_2O_3 NMQL is better than that under MoS_2. This result reflects that, given the same viscosity of nanofluid, the lubrication performance is better when nanoparticles are closer to spheres. SiO_2 and Al_2O_3 nanoparticles are spheres, but SiO_2 NMQL gains the best workpiece surface quality. This finding demonstrates that, given a similar structure, higher viscosity contributes a better lubrication effect.

5 Conclusion

The lubrication performance of six different nanofluids (Al_2O_3, MoS_2, SiO_2, CNTs, SiC, and graphite) for MQL milling Ti alloy was discussed on the basis of experimental research by analyzing the performance of milling parameters

(i.e., milling force, friction coefficient, surface roughness, energy spectrum of workpiece surface, and surface microstructure of debris and workpiece). The physicochemical properties of nanoparticles and the viscosity analysis of nanofluids were also explained. The conclusions drawn are as follows.

(1) MQL acquires the highest force ($F_x = 348$ N, $F_y = 202$ N) and friction coefficient ($\mu = 0.79$), followed by graphite NMQL ($F_x = 330$ N, $F_y = 179$ N, $\mu = 0.633$), and Al_2O_3 NMQL presents minimum values ($F_x = 312$ N, $F_y = 96$ N, $\mu = 0.413$). Specific energy has a consistent variation trend with that of milling force. Hence, Al_2O_3 NMQL claims the lowest energy consumption and conforms to the requirements on environmental protection and efficiency.

(2) MQL gains the highest surface roughness value ($R_a = 1.596$ μm, $RS_m = 0.399$ mm). In NMQL, SiO_2 NMQL gains the lowest R_a value (0.594 μm), whereas SiC NMQL gains the highest one (0.94 μm). Al_2O_3 NMQL has the lowest RS_m value (0.095 mm), whereas graphite NMQL has the highest one (0.295 mm). Workpiece surface shape parameters (R_{mr}) under Al_2O_3 and SiO_2 NMQL are analyzed. The workpiece surface under SiO_2 NMQL has few heaves, large profile valleys, and high oil storage capacity, which indicate the best workpiece surface quality under this working condition.

(3) The analysis of the surface microstructures of debris and workpiece demonstrates that the debris under MQL and graphite NMQL is C shaped, whereas the debris under other working conditions is helical curled. The back of debris under Al_2O_3 NMQL is the smoothest, and the morphology is improved remarkably. The workpiece surfaces under SiC and graphite NMQL have the thickest scratches in nanofluid milling, whereas the workpiece surface under SiO_2 NMQL shows the thinnest scratches and the highest smoothness. The EDS analysis presents that the Al content on the workpiece surface under Al_2O_3 NMQL is high, which forms the element deposition on the workpiece surface to form the lubrication film. The lubrication performance is improved.

(4) The analysis of the physicochemical properties of nanoparticles and the viscosity of nanofluid show that spherical Al_2O_3 and SiO_2 nanoparticles can improve the lubrication performance of base oil mostly. Al_2O_3 nanoparticles have the highest hardness, and they are beneficial to reducing milling force and specific energy. SiO_2 nanoparticles exhibit high viscosity, which is beneficial to forming a high workpiece surface quality.

Funding information This research was financially supported by the following foundation items: The National Natural Science Foundation of China (51575290), Major Research Project of Shandong Province (2017GGX30135 and 2018GGX103044), Shandong Provincial Natural Science Foundation, China (ZR2017PEE002 and ZR2017PEE011), and Scientific Research Development Project of Shandong Higher Education Institutions, China (J17KB016).

References

1. Du SG, Lv C, Ren JX, Yang ZC (2008) Surface morphology and surface tissue study of titanium alloy TC4 high speed milling. Acta Aeronaut Astronaut Sin 29:1710–1715
2. Ulutan D, Ozel T (2011) Machining induced surface integrity in titanium and nickel alloys: a review. Int J Mach Tools Manuf 51: 250–280
3. Deng ZH, Zhang H, Fu YH, Wan LL, Lv LS (2018) Research on intelligent expert system of green cutting process and its application. J Clean Prod 185:904–911
4. Zhang JC, Li CH, Zhang YB, Yang M, Jia DZ, Hou YL, Li RZ (2018) Temperature field model and experimental verification on cryogenic air nanofluid minimum quantity lubrication grinding. Int J Adv Manuf Technol 97:209–228
5. Jia DZ, Li CH, Zhang YB, Yang M, Wang YG, Guo SM, Cao HJ (2017) Specific energy and surface roughness of minimum quantity lubrication grinding Ni-based alloy with mixed vegetable oil-based nanofluids. Precis Eng 50:248–262
6. Mao C, Sun XL, Huang H, Kang CW, Zhang MJ, Wu YQ (2016) Characteristics and removal mechanism in laser cutting of cBN-WC-10Co composites. J Mater Process Technol 230:42–49
7. Mao C, Zhang MJ, Zhang J, Tang K, Gan HY, Zhang GF (2015) The effect of processing parameters on the performance of spark plasma sintered CBN-WC-Co composites. J Mater Eng Perform 24:4612–4619
8. Li BK, Li CH, Zhang YB, Wang YG, Jia DZ, Yang M, Zhang NQ, Wu QD, Han ZG, Sun K (2017) Heat transfer performance of MQL grinding with different nanofluids for Ni-based alloys using vegetable oil. J Clean Prod 154:1–11
9. Hamdan A, Sarhan AAD, Hamdi M (2012) An optimization method of the machining parameters in high-speed machining of stainless steel using coated carbide tool for best surface finish. Int J Adv Manuf Technol 58:81–91
10. Zhang YB, Li CH, Jia DZ, Zhang DK, Zhang XW (2015) Experimental evaluation of the lubrication performance of MoS_2/CNT nanofluid for minimal quantity lubrication in Ni-based alloy grinding. Int J Mach Tools Manuf 99:19–33
11. Zhang YB, Li CH, Jia DZ, Zhang DK, Zhang XW (2015) Experimental evaluation of MoS_2 nanoparticles in jet MQL grinding with different types of vegetable oil as base oil. J Clean Prod 871:930–940
12. Li CH, Hou YL, Xiu SC, Cai GQ (2008) Application of lubrication theory to near-dry-green grinding-feasibility analysis. Adv Mater Res 44-46:135–142
13. Li CH, Li JY, Wang S, Jia DZ (2013) Modeling and numerical simulation of the grinding temperature distribution with nanoparticle jet of MQL. Adv in. Mech Eng 7:167–181
14. Li BK, Li CH, Zhang YB, Wang YG, Yang M, Jia DZ, Zhang NQ, Wu QD, Ding WF (2017) Numerical and experimental research on the grinding temperature of minimum quantity lubrication cooling of different workpiece materials using vegetable oil-based nanofluids. Int J Adv Manuf Technol 93:1971–1988
15. Han ZL, Li CH (2010) The application of cutting fluid in grinding process is reviewed. Abras Abras Commun 10:7–12
16. Yang M, Li CH, Zhang YB, Jia DZ, Zhang XP, Hou YL, Li RZ, Wang J (2017) Maximum undeformed equivalent chip thickness for

ductile-brittle transition of zirconia ceramics under different lubrication conditions. Int J Mach Tools Manuf 122:55–65
17. Zhang DK, Li CH, Zhang YB, Zhou DZ (2015) Zhang XW. Experimental research on the energy ratio coefficient and specific grinding energy in nanoparticle jet MQL grinding. Int J Adv Manuf Technol 78:1275–1288
18. Ding WF, Zhang LC, Li Z, Zhu YJ, Su HH, Xu JH (2017) Review on grinding-induced residual stresses in metallic materials. Int J Adv Manuf Technol 88:2939–2968
19. Ding WF, Barbara L, Zhu YJ, Li Z, Fu YC, Su HH, Xu JH (2017) Review on monolayer CBN superabrasive wheels for grinding metallic materials. Chin J Aeronaut 30:109–134
20. Mao C, Tang XJ, Zou HF, Huang XM, Zhou ZX (2012) Investigation of grinding characteristic using nanofluid minimum quantity lubrication. Int J Precis Eng Manuf 13:1745–1752
21. Mao C, Zhou X, Yin LR, Zhang MJ, Tang K, Zhang J (2016) Investigation of the flow field for a double-outlet nozzle during minimum quantity lubrication grinding. Int J Adv Manuf Technol 85:291–298
22. Mao C, Ren YH, Gan HY, Zhang MJ, Zhang J, Tang K (2015) Microstructure and mechanical properties of CBN-WC-Co composites used for cutting tools. Int J Adv Manuf Technol 76:2043–2049
23. Wang YG, Li CH, Zhang YB, Yang M, Li BK, Jia DZ, Hou YL, Mao C (2016) Experimental evaluation of the lubrication properties of the wheel/workpiece interface in minimum quantity lubrication (MQL) grinding using different types of vegetable oils. J Clean Prod 127:487–499
24. Li BK, Li CH, Zhang YB, Wang YG, Yang M, Jia DZ, Zhang NQ, Wu QD (2017) Effect of the physical properties of different vegetable oil-based nanofluids on MQLC grinding temperature of Ni-based alloy. Int J Adv Manuf Technol 89:3459–3474
25. Li BK, Li CH, Zhang YB, Wang YG, Jia DZ, Yang M (2016) Grinding temperature and energy ratio coefficient in MQL grinding of high-temperature nickel-base alloy by using different vegetable oils as base oil. Chin J Aeronaut 29:1084–1095
26. Zhang YB, Li CH, Ji HJ, Yang XH, Yang M, Jia DZ, Zhang XP, Li RZ, Wang J (2017) Analysis of grinding mechanics and improved predictive force model based on material-removal and plastic-stacking mechanisms. Int J Mach Tools Manuf 122:81–97
27. Hadi M, Atefi R (2015) Effect of minimum quantity lubrication with gamma-Al_2O_3 nanoparticles on surface roughness in milling AISID3 steel. Ind J Sci Technol 8:296–300
28. Shen B, Shih AJ, Tung SC (2008) Application of nanofluids in minimum quantity lubrication grinding. Tribol T 51:730–737
29. Mao C, Zou HF, Huang XM, Zhang JA Zhou ZX (2013) The influence of spraying parameters on grinding performance for nanofluid minimum quantity lubrication. Int J Adv Manuf Technol 64:1791–1799
30. Yin QA, Li CH, Zhang YB, Yang M, Jia DZ, Hou YL, Li RZ, Dong L (2018) Spectral analysis and power spectral density evaluation in Al_2O_3 nanofluid minimum quantity lubrication milling of 45 steel. Int J Adv Manuf Technol 97:129–145
31. Shen B, Kalita P, Malshe AP, Shih A (2008) Performance of novel MoS_2 nanoparticles based grinding fluids in minimum quantity lubrication grinding. Trans NAMRI/SME 36:357–364
32. Kalita P, Malshe AP, Kumar SA, Yoganath VG, Gurumurthy T (2012) Study of specific energy and friction coefficient in minimum quantity lubrication grinding using oil-based nanolubricants. J Manuf Process 14:160–166
33. Rahmati B, Sarhan AAD, Sayuti M (2014) Morphology of surface generated by end milling AL6061-T6 using molybdenum disulfide (MoS_2) nanolubrication in end milling machining. J Clean Prod 66: 685–691
34. Rahmati B, Sarhan AAD, Sayuti M (2014) Investigating the optimum molybdenum disulfide (MoS_2) nanolubrication parameters in CNC milling of AL6061-T6 alloy. Int J Adv Manuf Technol 70: 1143–1155
35. Uysal A, Demiren F, Altan E (2015) Applying minimum quantity lubrication (MQL) method on milling of martensitic stainless steel by using nano MoS2 reinforced vegetable cutting fluid. Procedia Soc Behav Sci 195:2742–2747
36. Dilbag S, Rao PV (2008) Performance improvement of hard turning with solid lubricants. Int J Adv Manuf Technol 38:529–535
37. Ming EO, Sayuti M, Sarhan AAD (2015) Fuzzy logic-based approach to investigate the novel uses of nano suspended lubrication in precise machining of aerospace AL tempered grade 6061. J Clean Prod 89:286–295
38. Sayuti M, Erh OM, Sarhan AAD, Hamdi M (2014) Investigation on the morphology of the machined surface in end milling of aerospace AL6061-T6 for novel uses of SiO_2 nanolubrication system. J Clean Prod 66:655–663
39. Sayuti M, Sarhan AAD, Hamdi M (2013) An investigation of optimum SiO_2 nanolubrication parameters in end milling of aerospace Al6061-T6 alloy. Int J Adv Manuf Technol 67:833–849
40. Peng DX, Kang Y, Hwang RM, Shyr SS, Chang YP (2009) Tribological properties of diamond and SiO_2 nanoparticles added in paraffin. Tribol Int 42:911–917
41. Sarhan AAD, Sayuti M, Hamdi M (2012) Reduction of power and lubricant oil consumption in milling process using a new SiO_2 nanolubrication system. Int J Adv Manuf Technol 63:505–512
42. Haddad Z, Abid C, Oztop HF, Mataoui A (2014) A review on how the researchers prepare their nanofluids. Int J Therm Sci 76:168–189
43. Zhang DK, Li CH, Jia DZ, Zhang YB, Zhang XP (2015) Specific grinding energy and surface roughness of nanoparticle jet minimum quantity lubrication in grinding. Chin J Aeronaut 28:570–581
44. Wang LJ, Guo CW, Ryuichiro Y, Wu Y (2009) Tribological properties of Mn–Zn–Fe magnetic fluids under magnetic field. Tribol Int 42:792–797
45. Zhang XP, Li CH, Zhang YB, Jia DZ, Li BK, Wang YG, Yang M, Hou YL, Zhang XW (2016) Performances of Al_2O_3/SiC hybrid nanofluids in minimum-quantity lubrication grinding. Int J Adv Manuf Technol 86(1–15):3427–3441
46. Zhang XP, Li CH, Zhang YB, Wang YG, Li BK, Yang M, Guo SM, Liu GT, Zhang NQ (2016) Lubricating property of MQL grinding of Al_2O_3/SiC mixed nanofluid with different particle sizes and microtopography analysis by cross-correlation. Precis Eng 47: 532–545
47. Lee CG, Hwang YJ, Choi YM, Lee JK, Choi C, Oh JM (2009) A study on the tribological characteristics of graphite nano lubricants. Int J Precis Eng Manuf 10:85–90
48. Alberts M, Kalaitzidou K, Melkote S (2009) An investigation of graphite nanoplatelets as lubricant in grinding. Int J Mach Tools Manuf 49:966–970
49. Huang HD, Tu JP, Gan LP, Li CZ (2006) An investigation on tribological properties of graphite nanosheets as oil additive. Wear 261:140–144
50. Shaji S, Radhakrishnan V (2003) Application of solid lubricants in grinding: investigations on graphite sandwiched grinding wheels. Mach Sci Technol 7:137–155
51. Shaji S, Radhakrishnan V (2003) Analysis of process parameters in surface grinding with graphite as lubricant based on the Taguchi method. J Mater Process Technol 141:51–59
52. Wang YG, Li CH, Zhang YB, Yang M, Li BK, Jia DZ, Hou YL, Mao C (2016) Experimental evaluation of the lubrication properties of the wheel/workpiece interface in minimum quantity lubrication (MQL) grinding using different types of vegetable oils. Tribol Int 127:487–499
53. Miguélez MH, Soldani X, Molinari A (2013) Analysis of adiabatic shear banding in orthogonal cutting of Ti alloy. Int J Mech Sci 75: 212–222

54. Junior ASA, Sales WF, Silva RBD, Costa ES, Machado AR (2017) Lubri-cooling and tribological behavior of vegetable oils during milling of AISI 1045 steel focusing on sustainable manufacturing. J Clean Prod 156:635–647
55. Wang YG, Li CH, Zhang YB, Yang M, Zhang XP, Zhang NQ, Dai JJ (2017) Experimental evaluation on tribological performance of the wheel/workpiece interface in minimum quantity lubrication grinding with different concentrations of Al_2O_3 nanofluids. J Clean Prod 142:3571–3583
56. Feng J (2009) Study on mechanism of Ti6Al4V high speed machining under different cooling lubrication conditions. Shan Dong University, Jinan, pp 35–38
57. Liu GT, Li CH, Zhang YB, Yang M, Jia DZ, Zhang XP, Guo SM, Li RZ, Zhai H (2018) Process parameters optimization and experimental evaluation for nanofluid MQL in grinding Ti-6Al-4V based on grey relational analysis. Mater Manuf Process 33:950–963
58. Xu D, Feng P, Li W, Ma Y, Liu B (2014) Research on chip formation parameters of aluminum alloy 6061-T6 based on high-speed orthogonal cutting model. Int J Adv Manuf Technol 72:955–962
59. Sun J, Guo YB (2008) A new multi-view approach to characterize 3D chip morphology and properties in end milling titanium Ti-6Al-4V. Int J Mach Tools Manuf 48:1486–1494
60. Velasquez JDP, Bolle B, Chevrier P, Geandier G, Tidu A (2007) Metallurgical study on chips obtained by high speed machining of a Ti-6 wt.%Al-4 wt.%V alloy. Mater Sci Eng A 452:469–474
61. Ge X, Xia Y, Cao Z (2015) Tribological properties and insulation effect of nanometer TiO_2 and nanometer SiO_2 as additives in grease. Tribol Int 92:454–461
62. Jia DZ, Li CH, Zhang DK, Wang S, Hou YL (2014) Investigation into the formation mechanism and distribution characteristics of suspended microparticles in MQL grinding. Recent Pat Mech Eng 7:52–62
63. Tao X, Jia ZZ, Kang X (1996) The ball-bearing effect of diamond nanoparticles as an oil additive. J Phys D Appl Phys 29:2932–2937
64. Rapoport L, Leshchinsky V, Lvovsky M, Nepomnyashchy O, Volovik Y, Tenne R (2002) Mechanism of friction of fullerenes. Ind Lubr Tribol 54:171–176
65. Rapoport L, Leshchinsky V, Lvovsky M, Lapsker I, Volovik Y, Feldman Y, Popovitz-Biro R, Tenne R (2003) Superior tribological properties of powder materials with solid lubricant nanoparticles. Wear 255:794–800
66. Kao MJ, Lin CR (2009) Evaluating the role of spherical titanium oxide nanoparticles in reducing friction between two pieces of cast iron. J Alloys Compd 483:456–459
67. Rahim EA, Sasahara H (2011) A study of the effect of palm oil as MQL lubricant on high speed drilling of titanium alloys. Tribol Int 44:309–317
68. Wang YG (2016) Tribological performance and experimental study of the wheel/workpiece interface in MQL grinding using nanofluids. Qingdao University of Technology, Qingdao
69. Zhang YB, Li CH, Jia DZ, Li BK, Wang YG, Yang M, Hou YL, Zhang XW (2016) Experimental study on the effect of nanoparticle concentration on the lubricating property of nanofluids for MQL grinding of Ni-based alloy. J Mater Process Technol 232:100–115
70. Kalin M, Kogovšek J, Remškar M (2012) Mechanisms and improvements in the friction and wear behavior using MoS_2 nanotubes as potential oil additives. Wear 280:36–45
71. Yu HL, Xu Y, Shi PJ, Wang HM, Wei M, Zhao KK, Xu BS (2013) Microstructure, mechanical properties and tribological behavior of tribofilm generated from natural serpentine mineral powders as lubricant additive. Wear 297:802–810
72. Wang YG, Li CH, Zhang YB, Li BK, Yang M, Zhang XP, Guo SM, Liu GT (2016) Experimental evaluation of the lubrication properties of the wheel/workpiece interface in MQL grinding with different nanofluids. Tribol Int 99:198–210
73. Sridharan U, Malkin S (2009) Effect of minimum quantity lubrication (MQL) with nanofluid on grinding behavior and thermal distortion. Trans NAMRI/SME 37:629–636
74. Shen B, Shih AJ (2009) Minimum quantity lubrication (MQL) grinding using vitrified CBN wheels. Trans NAMRI/SME 37: 129–136
75. Guo SM, Li CH, Zhang YB, Wang YG, Li BK, Yang M, Zhang XP, Liu GT (2016) Experimental evaluation of the lubrication performance of mixtures of castor oil with other vegetable oils in MQL grinding of nickel-based alloy. J Clean Prod 140:1060–1076
76. Sia SY, Bassyony EZ, Sarhan AAD (2014) Development of SiO_2 nanolubrication system to be used in sliding bearings. Int J Adv Manuf Technol 71:1277–1284
77. Li CH (2018) Theory and key technology of nanofluid minimum quantity grinding. Science Press, Beijing, pp 199–214